Fluid flow and heat transfer characteristics in a stirred cell system for crude oil fouling

M. Yang*, A. Young, and B. D. Crittenden

Department of Chemical Engineering
University of Bath, Bath, UK, BA2 7AY
*corresponding author: my223@bath.ac.uk

Abstract: A small (1 litre) batch stirred cell which is operated at temperatures up to 400^{o}C and pressures up to 30 bar is used to study fouling behaviours of selected crude oils. Comsol Multiphysics package is used for the CFD and heat transfer modeling for this stirred cell system. The simulation results are validated against the measured temperature data at various axial positions on the heated test probe. The Comsol simulation provides details of the fluid flow and heat transfer characteristics, which help to get better understanding of the fouling behavious in the stirred cell. Moreover, with the Comsol predicted surface temperature profile together with the fouling deposit thickness profile measured by Proscan technique, it becomes possible to correlate, for a fixed surface shear stress, the local fouling rate against the local surface temperature, and hence to obtain an Arrhenius plot from one experimental run.

Keywords: Crude oil fouling, CFD Heat transfer simulation.

1. Introduction

Crude oil fouling in the heat exchanger is one of the major causes of refinery energy inefficiency. This led to a number of investigations over a few decades, focusing on the parameters that govern rates of fouling, namely temperature, shear stress in particular. Eaton and Lux's [1, 2] batch stirred cell system is relatively compact, and uses much less volume of crude oil for experiments than recirculating flow loops [3], permitting easy extraction of samples for analysis without destruction of any of its parts after a test run. In this work, therefore, a batch stirred cell system constructed based on information in the original patent [1] has been used to obtain fundamental experimental data with selected crude oil samples.

However the lack of knowledge on surface temperature and shear stress distribution over the surface of the fouling test probe may result in poor understanding of the fouling behaviours, and hence, significantly limit the application potential of the stirred cell system. To obtain this essential knowledge, in the present study a commercial software package, Comsol Ver.3.4 (Comsol Inc, Burlington, MA, USA), has been used to model the distributions of fluid velocity, shear stress, surface temperature and heat flux over the batch stirred cell's heated test probe. The Comsol CFD package offers user-friendly graphic interfaces for the fluid property and boundary condition settings. Some of the CFD simulation results, notably temperature, can be validated against the measured temperature data at various axial positions on the heated test probe.

2. Modeling of the fluid flow and heat transfer in the stirred cell

2.1. The stirred cell system

A general arrangement of the batch stirred cell is shown in Fig. 1. Details of its construction and operation are provided by Young *et. al.* [4]. The cell comprises a pressure vessel, an upwards pointing test probe heated internally by a cartridge heater, a cylindrical stirrer mounted co-axially with the test probe and driven via a magnetic drive by an electric motor, an internal cooling coil, external surface band heaters, and a pressure relief system. There is a single thermocouple to measure the crude oil bulk temperature and two thermocouples, twb and tws, are located within the walls of the test probe. The cell is filled with about 900 mL of the crude oil, pressurized with nitrogen.

2.2. Model geometry and governing equations

For the purposes of simplicity, the batch stirred cell geometry is taken to be two-

dimensional with axial symmetry, as shown in Fig. 2, which shows also the modeling result of the temperature field. For simplicity, the six blue cycles near the wall represent the coiling coil and the small gap in the top of rotating stirrer represents one of its four vent holes.

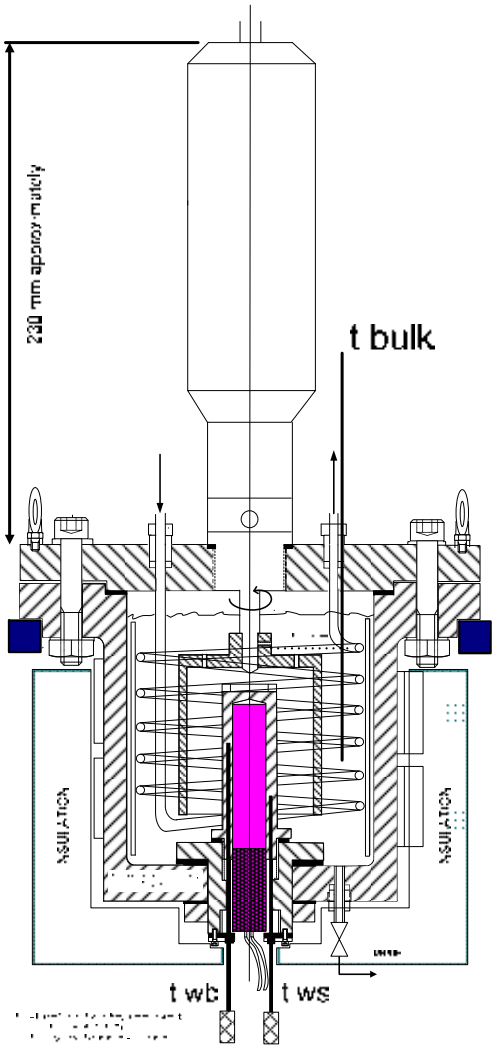

Fig. 1 The stirred cell system

The model tree consists of the turbulent swirl flows for the oil and gas phases respectively, heat conduction and convection in the fluid phases including the moving cap together with heat conduction in the stationary phases. For the turbulent flow k- ε model, the basic equations of continuity and momentum are in similar forms to normal Navier-Stokes equations. To describe the turbulence, the equations of the turbulent kinetic energy (k) and its dissipation rate (ε) are introduced as follows [5]:

$$\frac{\partial(\rho k)}{\partial t}+\rho u\cdot\nabla k=\nabla\cdot\left[\left(\eta+\frac{\eta_T}{\sigma_k}\right)\nabla k\right]+\eta_T\left[\nabla u+(\nabla u)^T\right]^2-\rho\varepsilon$$

$$\frac{\partial(\rho \varepsilon)}{\partial t}+\rho u\cdot\nabla\varepsilon=\nabla\cdot\left[\left(\eta+\frac{\eta_T}{\sigma_\varepsilon}\right)\nabla \varepsilon\right]+\rho C_{\varepsilon 1} C_\mu k\left[\nabla u+(\nabla u)^T\right]^2-\rho C_{\varepsilon 2}\frac{\varepsilon^2}{k}$$

Here, $\eta_T = \rho C_\mu k^2/\varepsilon$ is the turbulent dynamic viscosity. Values of the k-ε model parameters are cited from Comsol manual [5].

For the heat transfer equations, the turbulence results in an effective thermal conductivity k_{eff} [6]:

$k_{eff} = k_o + k_T$
$k_T = C_p\eta_T$

The physical property data for each crude oil are obtained from the supplier and from the literature [7, 8]. The physical data of some common materials, such as stainless steel and nitrogen involved in the model are taken from Comsol built-in material library.

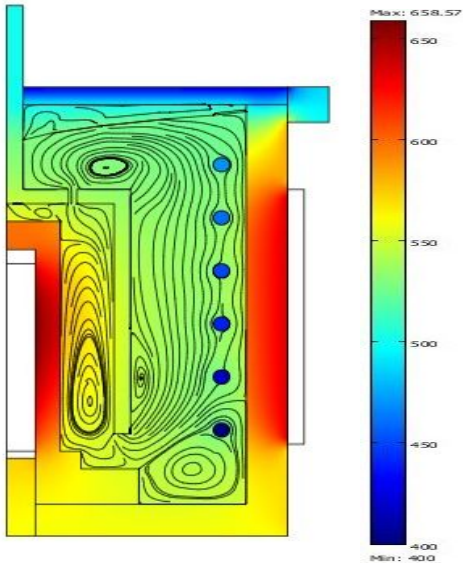

Fig. 2. Model scheme and the resulted flow streamline and temperature field of the stirred cell Crude B
Stirring speed: 200rpm
Heat power: 500W, average heat flux 106kW/m^2

2.3. Boundary conditions

The boundaries in the swirl flow subdomains are set to be logarithmic wall functions for the fluid and stationary walls, moving wall for the fluid and the rotating stirrer wall. For the heat transfer, the boundary conditions are set to be a thermal wall function for the fluid side and a heat flux for the wall side including the coil wall, thermal insulation for the top, bottom, and side walls. The heat flux through the wall of the heated probe was set according to the power Applied.

2.4. Oil and gas interface simulation

The fluid is going through an initial transient period because of the weight and swirl centrifuge effects, until the interface of the oil and gas becomes stable. This initial transient simulation was carried out using the level set method [9]. A level set function ϕ is introduced to define the interface, where ϕ = 0.5. The ϕ equation is as follows:

$$\frac{\partial \phi}{\partial t} + u \cdot \nabla \phi = \gamma \nabla \cdot (-\phi(1-\phi)\frac{\nabla \phi}{|\nabla \phi|} + \varepsilon \nabla \phi$$

The body forces are gravity and centrifuge forces, which is in terms of $\rho w^2/r$. A time dependence solver is used to solve the function ϕ. Fig. 2 shows the simulated gas and liquid interface which is leaning toward the wall as expected for the swirl flow.

2.5. Solver parameter for CDF and heat transfer simulation

The simulation of the steady state of fluid flow and heat transfer in the stirred cell was carried out using stationary solver. It was found that a gradual approach to the designed operation parameter, namely the stirring speed in rpm, was necessary for the solution to converge. A factor is used to allow the simulation to start with low stirring speed, 100rpm for instance, and then increase stepwise up to 500rpm. This was implemented by setting the boundary conditions of the moving stir wall velocity to be a function of rpm as follows:

$$\varphi = 2\pi r \frac{rpm}{60}$$

Where rpm is the rotation speed of the stir cap, and r is the radius of the wall. The simulation conducted this way provides solutions for a series of stirring speed in a single computing run.

3. Results and discussion

3.1. Velocity, turbulent viscosity and shear stress distribution

Fig. 3 shows that simulated velocity distribution along the radius from the probe surface to the stir cap inner wall at a middle vertical location (z = 0.04m). It is observed from the curves that the velocity gradient increases as the rpm.

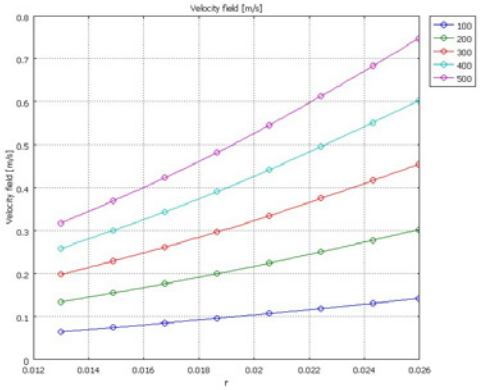

Fig. 3 Velocity radius distribution
Stirring speed: 100 – 500 rpm
Heater power: 500W

Fig. 4 shows the turbulent viscosity radius distribution, and Fig. 5 shows the turbulent viscosity vertical distribution over the probe surface. It is seen that the turbulent viscosity increases as the rpm increases. The value of the turbulent viscosity is as high as two orders of the molecular viscosity, hence the shear stress would be mainly determined by the turbulent viscosity and the velocity gradient.

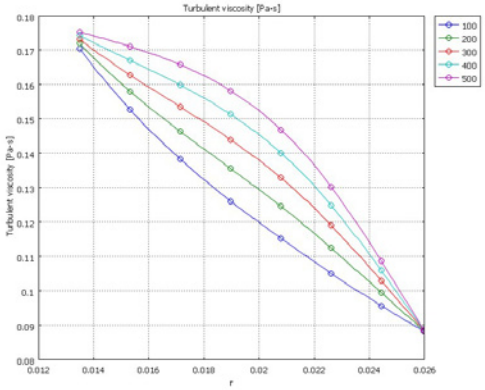

Fig. 4 Turbulent viscosity radius distribution
Stirring speed: 100 – 500 rpm
Heater power: 500W

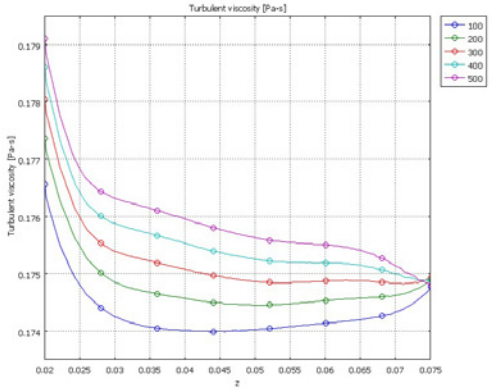

Fig. 5 Turbulent viscosity distribution over the probe surface
Stirring speed: 100 – 500 rpm
Heater power: 500W

Fig. 6 shows the shear stress distributions along the heated probe surface as a function of the stirrer speed for a power of 500W and average heat flux of 106 kW/m^2. As expected, the surface shear stress on the heated probe surface is reduced as the stirrer speed is reduced.

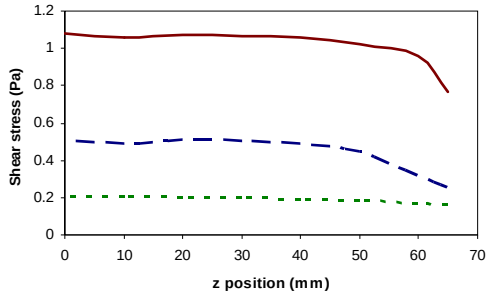

Fig. 6. Shear stress along the probe surface
Upper line: 400rpm
Mid line: 200rpm
Lower line: 100rpm

3.2. Temperature distribution

Fig. 2 shows the CFD-simulated temperature field in both the solid and fluid phases for Crude B with the operating conditions shown in the caption to this figure. Fig. 7 shows the temperature radius distribution in the middle vertical section (z = 0.04m) at stirring speed from 100 to 500rpm. Clearly, the higher stirring speed enhances the heat transfer, resulting in lower temperature at given locations.

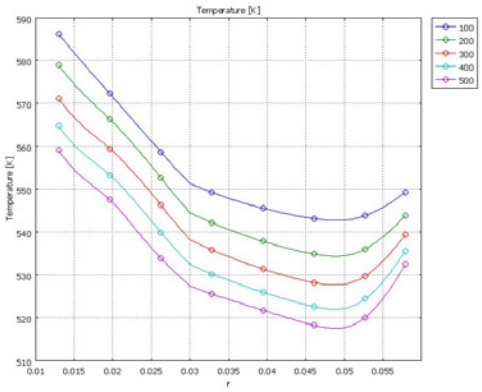

Fig. 7 Temperature radius distribution

Fig. 8 shows the temperature distribution over the probe surface and over the radius position where the two surface (wall) thermocouples, denoted by T_{wb} and T_{ws}, are located. The good agreement between the actual measurements for T_{wb} and T_{ws} and their model predicted values using Comsol helps to validate the simulation.

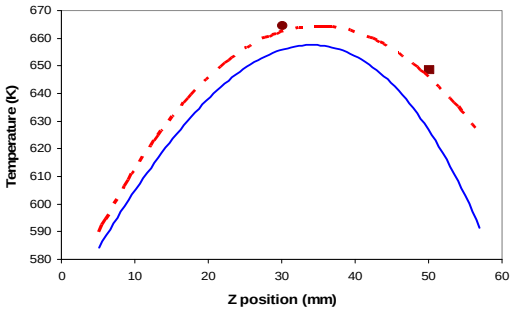

Fig. 7. Temperature distribution
Blue line: Temperature of the probe surface
Red dash line: Temperature at the imagined cylinder surface, where the two thermocouples located

3.3 Effect of surface temperature and the shear stress on the fouling behaviour

In general, the fouling rate in the batch stirred cell depends on the stirring speed and hence on the shear stress when the surface temperature is kept the same. An increase in the stirring speed from 200 to 400 rpm increases the shear stress from 0.52 Pa to 1.17 Pa and causes the fouling rate to be reduced from 0.016

$m^2K/(kWh)$ to 0.0054 $m^2K/(kWh)$. Details of the experimental results of the fouling rate are provided by Young *et. al*. [4].

For a fouling experiment at fixed stirring speed, the fouling rate is basically determined by the surface temperature, and in general, the higher the temperature, the higher the fouling rate.

As shown in Fig. 6, at a fixed stirring speed the shear stress over the probe surface is relatively constant except the very bottom section. Hence the fouling behaviour is solely determined by the surface temperature since the shear stress is more-or-less constant. As shown in Fig. 8 the surface temperature reaches peak at the middle section of the probe and gradually decreases in both top and bottom directions. With such a surface temperature profile, the fouling rate over the probe surface would be expected to vary in the same manner. This prediction is well supported by the experimental results.

Given the nearly constant fouling rate over the running time after the induction period and the same running time regardless of the position on the probe surface [4, 10], the fouling rate at a particular location on the probe surface can be expressed in terms of the local fouling deposit thickness. The fouling deposit thickness was measured using a micro optical scan technique, Proscan [4], and its profile over the probe surface is shown in Fig. 9. The Comsol model predicted temperature profile over the probe surface is also plotted in Fig. 9 and can be compared with the deposit thickness profile.

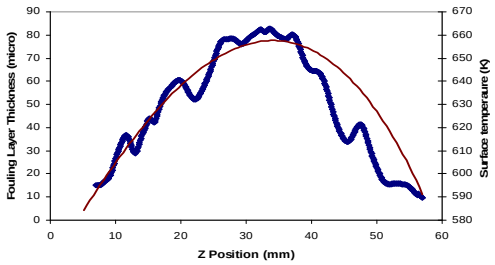

Fig. 9 Fouling layer thickness and simulated surface temperature profiles

Blue symbols: fouling layer thickness by Proscan; red line: surface temperature by Comsol simulation

3.4. Arrhenius plot

Given the local fouling rate expressed in terms of the local fouling deposit thickness, the Arrhenius plot can therefore be taken in terms of logarithm of the fouling layer thickness, *x*, as a function of the inverse of the absolute surface temperature, *T*:

$$ln\ x = A - E_A/RT \tag{10}$$

Here, A is the pre-exponential factor and E_A is the apparent activation energy, as described by Crittenden *et. al*.[3]. The Arrhenius plot is shown in Fig. 10, from which the apparent activation energy of 60.7 kJ/mol can be obtained for Petronas B crude oil subjected to a power of 500W, a heat flux of 106 kW/m^2 and a bulk temperature of 260°C over 33 hours of total running time in the batch stirred cell.

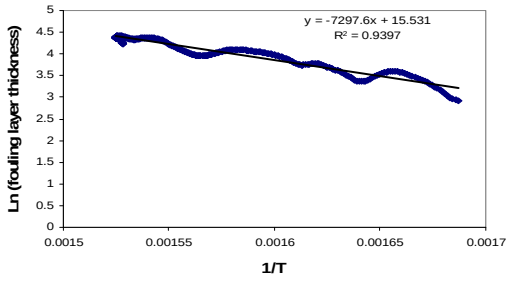

Fig. 10 Arrhenius plot for Crude B

Unlike the more usual Arrhenius plots obtained for fouling experiments, this Arrhenius plot (Fig. 10) is in a continuous form, demonstrating the clear advantage of using the batch stirred cell in conjunction with both the Comsol simulation for surface temperature and the Proscan technique for deposit thickness. In most other crude oil fouling experiments, a minimum of three to four separate experiments at different surface temperatures need to be carried out in order to obtain a few points to construct an Arrhenius plot.

4. Conclusions

CFD and heat transfer simulations for a batch stirred cell system have been carried out using Comsol and validated partially against the

measured temperature data at various axial positions on the heated test probe. The surface temperature and shear stress profiles which are predicted by the CFD model help to get better understanding of the fouling behaviour in the batch stirred cell system.

The model simulation using Comsol together with the practical fouling deposit thickness measurement using Proscan makes it possible to correlate, for a relatively fixed surface shear stress, the local fouling rate against the local surface temperature, and hence to obtain an Arrhenius plot from one experimental run. This approach significantly enhances the application potential of the simple batch stirred cell fouling test system.

Acknowledgements

The authors are grateful to the UK's Engineering and Physical Sciences Research Council (EPSRC) for the award of a research grant (EP/D506131/1) to study the role of asphaltenes in crude oil fouling. The authors are grateful also to their EPSRC project partners at Imperial College London and the University of Cambridge, as well as to ExxonMobil and Petronas who supplied samples of crude oils.

Reference

1. Eaton, P., Fouling test apparatus, US patent 4383438 (1983).
2. Eaton, P. and Lux, R., 1984, Laboratory fouling test for hydrocarbon feed-stocks, ASME-HTD, Vol. 35, pp. 33-42 (1984).
3. Crittenden, B. D., Kolaczkowski., S. T. and Phillips D. Z., Crude oil fouling in a pilot-scale parallel tube apparatus, *Heat Transfer Engineering*, Vol. 30(10-11), pp. 777-785 (2009).
4. Young, A., Venditti, S., Berrueco, C., Yang, M., Waters, A., Davies, H., Millan, M. and Crittenden, B. D., Characterisation of crude oils and their fouling deposits, accepted to be included in *Proc. 8th International Conference on Heat Exchanger Fouling and Cleaning: Challenges and Opportunities*, Schladming, Austria, 14-19 June, 2009.
5. Comsol, Model library - chemical engineering module, pp. 237-240 (2006).
6. Comsol, Model library - chemical engineering module, pp. 230-231 (2006).
7. ASTM D341, 2003, Standard test method for viscosity-temperature charts for liquid petroleum products, ASTM International.
8. Nelson, W. L., Petroleum Refinery Engineering, 4th edition, McGraw-Hill, New York, pp 169 and 530 (1958).
9. Comsol, Model library - chemical engineering module, pp. 201-215 (2006).
10. Yang, M, Young, A, Niyetkaliyev, A. and Crittenden, B. D., Modeling of the induction period of crude oil fouling. accepted to be included in *Proc. 8th International Conference on Heat Exchanger Fouling and Cleaning: Challenges and Opportunities*, Schladming, Austria, 14-19 June, 2009.